

# Speckle Simulation Tool for the Design of Laser-based Displacement Sensors

Ernst Csencsics, Tobias Wolf, and Georg Schitter

Automation and Control Institute (ACIN), Technische Universität Wien, Vienna, Austria

## ABSTRACT

This paper presents the development of a versatile, accurate and efficient speckle simulation tool for the design of laser-based displacement sensors, capable of handling objective as well as subjective speckles. The simulation tool integrates the statistical nature of speckles with the deterministic properties of ray-tracing simulations, providing a reliable estimation of the performance of laser and/or speckle-based sensors in the design phase, even for more complex optical assemblies. It enables the calculation of several simulation outputs in order to determine the best performing system configuration for a given requirement and measurement principle. To validate the simulation results, they are compared against the experimental data of four designed laser-speckle based sensor setups for measuring in- and out-of-plane displacement of a target as well as against analytical relations for describing speckle pattern translation for simple geometries. With resulting simulation errors of less than  $2\text{ }\mu\text{m}$  rms for in-plane (output: correlation peak shift) and  $2.6\text{ }\mu\text{m}$  for out-of-plane displacements (output: center of gravity shift) for an integrated laser sensor geometry, the good accuracy of the speckle simulation tool is demonstrated.

**Keywords:** Laser speckles, Speckle simulation, Triangulation sensor, Displacement measurement, Surface tracking, In-process measurement, Design tool

## 1. INTRODUCTION

Numerous applications in science and industry require accurate tracking of an object surface by a respective tool for enabling high precision measurements or manipulations on a moving target or product piece. They range from medicine and life sciences<sup>1,2</sup> all the way to manufacturing.<sup>3,4</sup> A particular application case, which is of highest interest for the manufacturing industry, are robot-based high resolution 3D inline measurements,<sup>5</sup> where the systems need to actively track the motion of the target with single micrometer precision, compensating for vibrations of the production environment in all six degrees of freedom.<sup>3,6</sup>

While there are plenty of optical principles, such as laser triangulation, available for measuring out-of-plane displacement,<sup>7</sup> laser speckle measurement principles are one of the most promising concepts for measurements of in-plane displacement. They offer advantages such as high resolution, contact-less measurements and applicability to most technical surfaces without the need for additional markers.<sup>8</sup> Due to the limited measurement range caused by decorrelation, they have so far been mainly used for strain measurements in the past.<sup>9,10</sup> To overcome this drawback, advanced concepts have been introduced to make them also applicable for measuring tool speeds,<sup>11</sup> as well as the relative<sup>12</sup> and absolute position of a target.<sup>13</sup> Recently, a compensation-based laser sensor has been proposed for tracking translational in- and out-of-plane displacement of a target. It integrates principles of laser triangulation and objective laser speckle measurement into a single device, providing an in-plane and out-of-plane resolution of single micrometers.<sup>14</sup>

The design of such integrated sensors as well as the assessment of the impact of speckle effects on the uncertainty of laser based sensors is, however, challenging,<sup>15</sup> as there are hardly any versatile simulation tools available that can be employed to estimate the performance of non-trivial sensor geometries. Existing approaches focus mostly on the statistical nature of speckle patterns by employing 2D Fast Fourier Transforms to generate

---

Further author information: (Send correspondence to Ernst Csencsics)

Ernst Csencsics: E-mail: [csencsics@acin.tuwien.ac.at](mailto:csencsics@acin.tuwien.ac.at), Telephone: +43 (0)1 588 01-376 524

artificial speckle patterns,<sup>16</sup> the Fourier shift theorem to describe in-plane translation<sup>17</sup> or provide numerical simulations of dynamic speckle sequences to analyze transients of e.g. paint drying processes.<sup>18</sup>

This paper proposes a versatile, accurate and efficient speckle simulation tool for the design of laser-based displacement sensors. By integrating the statistical nature of speckles with the deterministic properties of ray-tracing simulations, the tool is capable of handling objective as well as subjective speckles. It enables the calculation of several outputs, such as sensitivity or crosstalk, for designed geometric assemblies up front, in order to determine the best performing configuration for given system requirements. The simulation tool considers the system geometry including the location, orientation and size of the laser source, the target surface, the detector (with number and size of pixels) as well as apertures, lenses, or mirrors if applicable. To validate the results, the simulation output for various system geometries is compared against analytic relations for describing speckle displacement and decorrelation, as well as against experimentally acquired data. Section 2 introduces the fundamentals of speckle formation, followed by a description of the simulation procedure in Section 3. In Section 4 the experimental setup is introduced and the simulation output is validated against experimental data and analytic calculations. Section 5 concludes the paper.

## 2. FORMATION OF LASER SPECKLES

With an optically rough surface being illuminated by coherent light, each illuminated spot on the micro-structured surface can be considered as individual scatterer, scattering the incoming light randomly in direction, amplitude and phase. The scattered waves propagate away from the surface while interfering with each other. Imaging this interference effect as a spatial intensity distribution with an objective or in the diffraction field, a grainy pattern of bright and dark spots, termed laser speckle pattern, is obtained.<sup>19</sup> When using a focused lens system, as with a typical laser triangulation sensor, subjective laser speckles (SLSPs) can be observed, with the aperture limiting the spatial interaction of the individual waves emerging from the surface.<sup>8</sup> When no imaging system is used (free space observation) objective laser speckle (OLSP) patterns are observed, with the entire illuminated area contributing to the resulting speckle pattern. The lens-less case with OLSPs enables in general more compact sensor designs and avoids lens aberrations.<sup>20</sup>

Figure 1 shows the configuration of an OLSP-based sensor system for measuring in-plane displacements along the x- and y-axis without imaging optics. Integrating a lens as imaging optics between target and observation plane would on the other hand entail the formation of SLSPs. A laser in the xz-plane is used to illuminate the

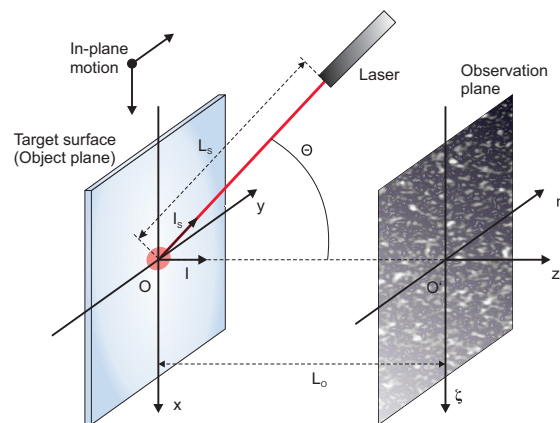


Figure 1. Laser speckle-based sensor configuration without imaging optics for measuring in-plane target displacement. Illumination of an optically rough target surface with a coherent laser beam leads to the formation of OLSPs in the observation plane. The in-plane displacement of the target results in a respective shift of the pattern (see (1) and (2)).

optically rough target surface. It is a distance  $L_S$  away from the origin  $O$  and tilted by an angle  $\Theta$  with respect

to the surface normal. The image detector is placed in the observation plane, which is parallel to the object plane (without loss of generality) and located at the distance  $L_O$ . Neglecting rotations and stress, the displacement of the speckle pattern in  $\zeta(x)$ - and  $\eta(y)$ -direction caused by a displacement of the target can be expressed by<sup>20</sup>

$$A_\zeta = -a_x \left[ \frac{L_O}{L_S} (l_{Sx}^2 - 1) + l_x^2 - 1 \right] - a_y \left[ \frac{L_O}{L_S} l_{Sx} l_{Sy} + l_x l_y \right] - a_z \left[ \frac{L_O}{L_S} l_{Sx} l_{Sz} + l_x l_z \right], \quad (1)$$

$$A_\eta = -a_x \left[ \frac{L_O}{L_S} l_{Sx} l_{Sy} + l_x l_y \right] - a_y \left[ \frac{L_O}{L_S} (l_{Sy}^2 - 1) + l_y^2 - 1 \right] - a_z \left[ \frac{L_O}{L_S} l_{Sy} l_{Sz} + l_y l_z \right] \quad (2)$$

with  $a_{x,y,z}$  the displacements of the target in the three translational DoFs. For the nominal case of a parallel object and observation plane the simplified unit vectors  $\vec{l} = (l_x, l_y, l_z)^T = (0, 0, 1)^T$  and  $\vec{l}_S = (l_{Sx}, l_{Sy}, l_{Sz})^T = (\sin(\Theta), 0, \cos(\Theta))^T$  given in Fig. 1 are obtained. If the two planes are not parallel, additionally small crosstalk terms need to be considered.

For estimating the speckle pattern displacement, the two-dimensional normalized cross-correlation function (NCC) is most commonly applied to the shifted version and a reference image.<sup>21</sup> A direct estimate for the spatial displacement is given by the position of the NCC peak value with a resolution of  $\pm 1/2$  pixel, without additional interpolation. The use of laser speckles for displacement measurement is always limited by decorrelation effects caused by three major factors: (i) changes in the microstructure due to stress or strain, (ii) the relative overlap of the correlation windows and (iii) changes of the illumination position on the surface due to target displacement. While strain is neglected for displacement measurements and the second factor can be decreased by interpolation,<sup>22</sup> the third factor can be overcome by compensation-based sensing systems.<sup>14</sup>

### 3. SIMULATION PROCEDURE

According to the problem statement, a versatile simulation tool for speckle effects should be capable of handling arbitrary system geometries, consider various optical elements and evaluate correlation-based shifts of the speckle pattern as well as center of gravity (CoG) shifts of a partly illumination of the detector area in order to calculate in- and out-of-plane displacements. The simulation tool provides these properties by integrating the statistical nature of laser speckles with the deterministic properties of the ray tracing method, making it suitable for a broad range of applications including optical sensors.

The basic implementation of the simulation tool and its algorithms is done in *MATLAB* (MathWorks Inc., MA, USA) using the *Optometrika* library,<sup>23</sup> which provides ray tracing functions together with a number of optical elements. The algorithm itself consists of two parts and is illustrated in the flowchart in Fig. 2. Part 1 (left column) starts with the definition of the system geometry including the location, orientation and size of the laser source, the target surface, the detector (with number and size of pixels) and apertures and/or lenses, if applicable. The laser spot on the target is approximated by  $N_1$  point sources, which are equally distributed within the spot diameter in x- and y-direction and randomly distributed within the expected surface roughness of the target material in z-direction. The related intensities of the point sources are normally distributed in order to resemble a Gaussian beam intensity profile (see Fig. 3a). Each of the  $N_1$  point sources (running index  $j$  in Fig. 2) is again approximated by  $N_2$  rays, which beam out equally distributed over a pre-set solid angle  $\Omega$ . Using the ray tracing functions of the *Optometrika* library, each of the emerging rays is propagated towards the detector through the previously defined optical system. All rays not intersecting with the pre-defined detector area, as they are for example blocked by an aperture as shown in Fig. 3b, are discarded for the further considerations. With the known optical path lengths and the used laser wavelength, the phase of each ray at the intersection point with the detector can be calculated. As not all detector pixels will be hit by a ray from a specific point source, grid data interpolation with a meshgrid according to the pixel size is employed to calculate possibly missing phase values. This sequence is repeated for all point sources, until the running index  $j$  reaches the value of  $N_1$ . Using the intensity and phase image matrix of each point source on the detector, the speckle image is calculated by complex superposition of all point sources.

With the calculation of the speckle pattern according to part 1 of the algorithm, part 2 takes care of the effects of in- and out-of-plane target displacements and the computation of the simulation outputs (see Fig. 2). A target translation is simulated via manipulating the laser point source positions according to the defined

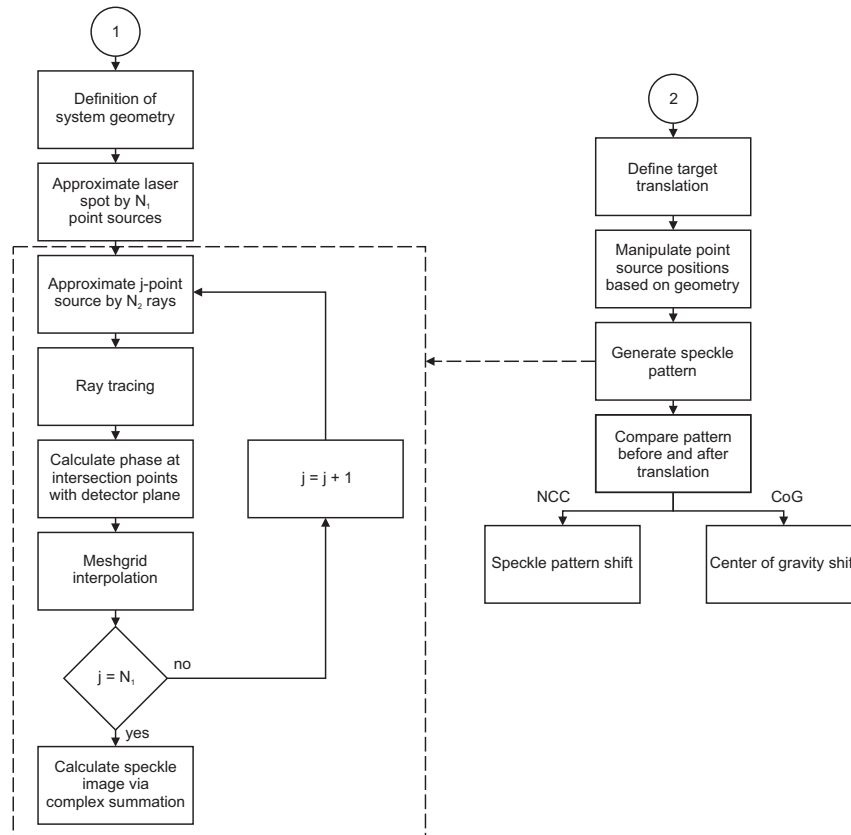


Figure 2. Flowchart of the simulation procedure. Part 1 shows the generation of the laser speckle image. Part 2 calculates the effects of translational target displacements on the resulting speckle pattern and derives application specific outputs, such as the NCC peak or CoG shift.<sup>14</sup>

geometry. For in-plane target displacements the absolute location of the illuminated area stays constant, while the positions of the point sources are laterally shifted according to the target displacement. For out-of-plane target displacements the positions of the point sources stay constant, while the absolute position of the illuminated area shifts laterally according to the laser orientation and system geometry. In both cases some of the point sources leave the illuminated spot area, which makes them essentially invalid, and are replaced by new ones, added to the currently illuminated area. After adapting the point source positions and the illuminated area on the surface, a new speckle image on the detector is generated according to part 1 (see dotted box in Fig. 2). Based on the updated speckle pattern, the reference image and respective outputs depending on the application, such as the NCC correlation peak and CoG shift, can be calculated.

The formation of a representative speckle pattern requires a minimum number of point sources for approximating the laser spot on the target, which should, however, be kept as small as possible for the sake of computational efficiency. In Fig. 4 the speckle pattern on the detector is shown for the basic OLSP setup configuration shown in Fig. 1 with an additional 1 mm aperture between target surface and observation plane.<sup>14</sup> The aperture and the detector are placed 39 mm and 78 mm away from the surface, respectively, with a detector size of 4.2 x 4.2 mm and a pixel size of 3 x 3  $\mu\text{m}$ . The distance between laser (wavelength of 632.8 nm) and surface is 50 mm and the angle  $\Theta$  is set to 30°. The number of point sources is varied from 1 over 4 to 100, using 1500 rays per point source for the subsequent ray tracing. Approximating the laser spot with a single point source leads to no interference effects on the detector. Increasing the number to 4 makes the effect of constructive and destructive interference

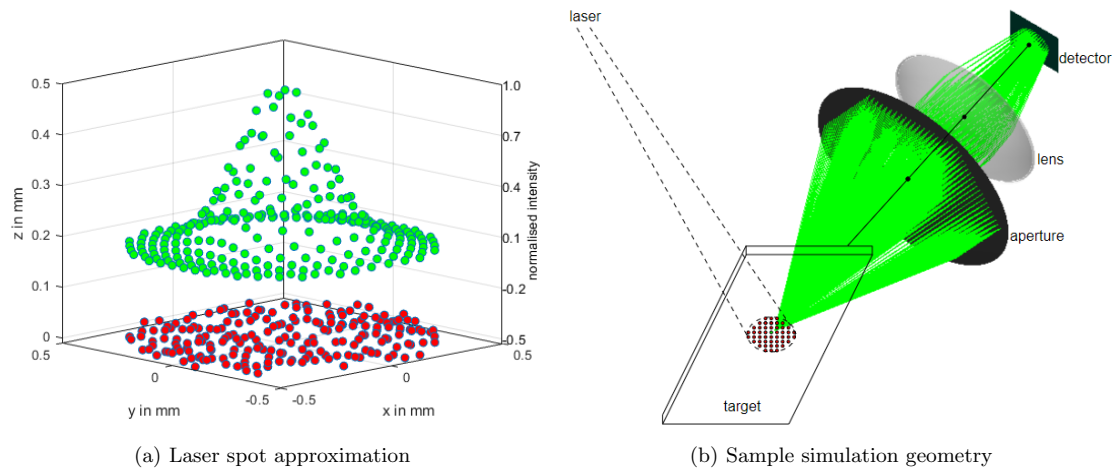


Figure 3. Simulation environment. (a) Approximation of the laser spot on the target with multiple point sources. The red dots are the point source positions in space, with the  $z$ -values randomly distributed within the surface roughness of the target material. The green dots represent the associated Gaussian distributed intensity. (b) Ray tracing through an example system, containing an aperture and a lens. The green point source is approximated by  $N_2$  rays, which beam out under a defined solid angle and enable the calculation of a phase image on the detector for each point source.

visible but generates a non sufficiently random pattern. The fringes for example represent regions where only two point sources interfere, while in the middle region with the rectangular pattern all 4 point sources interfere. Setting the number of point sources to 100 leads to a good approximation of a fully developed speckle pattern for the given case, which is validated by correlation experiments with experimental data.

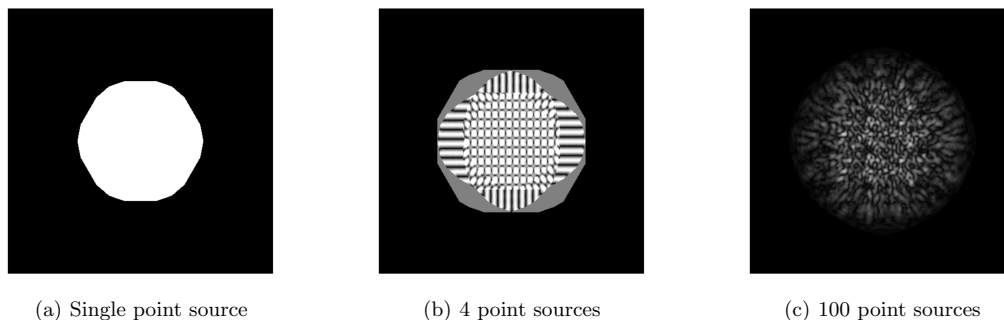


Figure 4. Simulated detector output for various numbers of point sources of an OLSP setup with additional aperture. (a) with a single point source no interference is obtained, while for (b) 4 point sources first constructive and destructive interference effects is observable. (c) 100 point sources lead to a fully developed speckle image.

#### 4. VERIFICATION OF SIMULATION RESULTS

In order to verify the results of the simulation tool as well as its capability to handle various system geometries, the output values for in- and out-of-plane displacements are compared against experimental measurements as well as analytic calculations.<sup>20</sup>

#### 4.1 Experimental setups

For the experimental investigation the four setups shown in Fig. 5 are used. The three simple OLSP setups (a)-(c), with available analytic formulas for describing the speckle pattern shifts, are used to assess the capability to handle various system geometries, while the setup with additional aperture (d), resembling the assembly of an integrated in- and out-of-plane sensor,<sup>14</sup> is used to test the consideration of additional optical components.

The setups are composed of a grey scale CMOS camera sensor (Type: DMK 22BUC03, Imaging Source GmbH, Germany) as detector with 744 x 480 pixels and a linear polarized HeNe laser (Model: 1108P, JDSU, CA, USA) with a wavelength of 632.8 nm, which is coupled into a single-mode fiber and directed towards the target, represented by a machined aluminium part with non-modified surface. In-plane (x-direction) and out-of-plane (z-direction) displacements of the target are realized with two stacked position controlled linear stages (Type: VT-80 62309120, Physik Instrumente (PI) GmbH, Germany) with a resolution of 500 nm. Further geometric parameters of the first three setups ((a)-(c)) include a laser distance to the target of 50 mm, a detector distance of 60 mm and an angle  $\Theta$  of  $35^\circ$ .

The fourth setup with additional aperture (d) is designed with slightly different geometric parameters for reasons of construction. The aperture is formed by an optical alignment target (SCPA1, Thorlabs Inc., NJ, USA) with a diameter of 1 mm and is added between target and detector, entailing a not fully illuminated detector area. The geometric parameters are set to a laser distance of 50 mm, a detector distance of 75 mm, an aperture distance of 41 mm and an angle  $\Theta$  of  $39^\circ$ . This configuration enables to distinguish between in- and out-of-plane displacements of the target within a certain range of motion, as out-of-plane target displacements transform into a CoG shift on the detector. The CoG shift due to out-of-plane displacement has a significantly higher sensitivity than the effects on the speckle pattern itself, such that the out-of-plane component can be determined by the CoG shift.<sup>14</sup> The image acquisition and processing is entirely done in *MATLAB* (MathWorks Inc., MA, USA), which is used to implement functions that calculate the NCC peak shift for all four setups ((a)-(d)) as well as the CoG shift for the last setup (d). A correlation window size is set to 64 x 64 pixel is used together with a two-fold interpolation, which leads to an experimental resolution of  $\pm 1/4$  pixel (i.e.  $3 \mu\text{m}$ ).

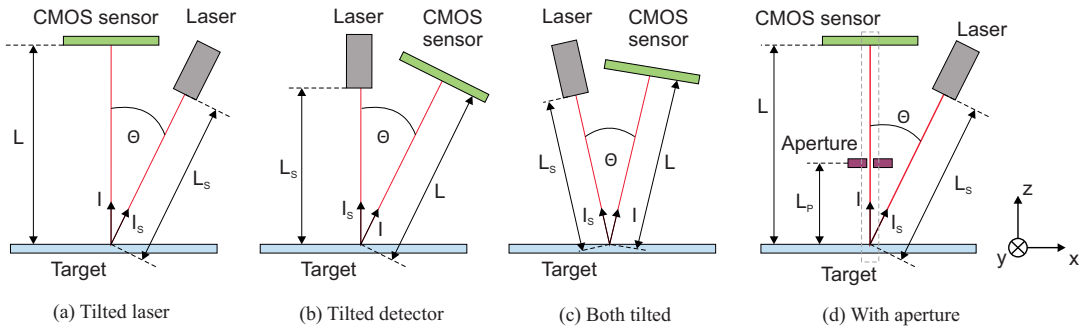


Figure 5. Configurations of experimental OLSP setups for verification of the simulation results. (a)-(c) are basic OLSP setup geometries for measuring in-plane displacement composed of a laser, a detector and the target itself. (d) is the configuration of an integrated laser sensor with additional aperture for measuring in- and out-of-plane displacement.

#### 4.2 Results

Performing subsequent quasi-static in- (x) and out-of-plane (z) target displacements and comparing simulation, measurement and analytic results, enables an evaluation of the simulation accuracy. For approximation of the laser spot 100 point sources and 1500 rays per point source are used (see Section 3). For reasons of efficiency, the simulation is done for 10 displacements over an entire range of  $200 \mu\text{m}$  and is linearly interpolated in-between, with the speckle pattern at  $0 \mu\text{m}$  serving as reference. With the used MATLAB implementation on a conventional personal computer, the simulation of a single displacement location takes about 90 s.

Considering the first setup with the tilted laser (a) as well as (1) and (2), the pattern displacement component in  $\eta$ -direction reduces to  $A_\eta = a_y(L_O/L_S + 1) = k_y \cdot a_y$ , so that there is no crosstalk from out-of-plane



displacements and the sensitivity  $k_y$  is independent of  $\Theta$ . For practical applications with large values of  $L_S$  the sensitivity  $k_y$  will always reside around 1.<sup>24</sup> The pattern displacement component in  $\zeta$ -direction reduces to  $A_\zeta = a_x [1 - L_O/L_S \cdot \cos^2(\Theta)] - a_z \cdot L_O/2L_S \cdot \sin(2\Theta)$ , showing a  $\Theta$ -dependent sensitivity  $k_x$  as well as a crosstalk component from out-of-plane motions, which gets diminished for decreasing values of  $\Theta$ . In Fig. 6 the resulting simulated, measured and analytically calculated NCC peak shifts are depicted as well as the simulation and measurement errors with respect to the analytically calculated, theoretical value. As expected the sensitivity, given by the ratio of the OLSP pattern shift to the target shift, of the assembly for in-plane displacements (see Fig. 6a) is about 1, while the crosstalk from out-of-plane target displacements on the speckle shift is as small as 5% for this setup (see Fig. 6b). The error of the measurement shows steps with heights of less than  $3 \mu\text{m}$ , which equals the resolution of the experimental setup (see section 4.1). Due to slightly diverging slopes the error increases towards larger displacements but stays well below one pixel size. The error of the in-plane simulation result shows a peak-to-valley (ptv) error of  $5.2 \mu\text{m}$  and a root-mean-square (rms) deviation of  $1.9 \mu\text{m}$ , giving a result even closer to the theoretical value than the measurement (error of  $11.1 \mu\text{m}$  ptv and  $2.5 \mu\text{m}$  rms). For out-of-plane displacement the obtained simulation result also matches the analytic result with an rms error of  $0.9 \mu\text{m}$  well.

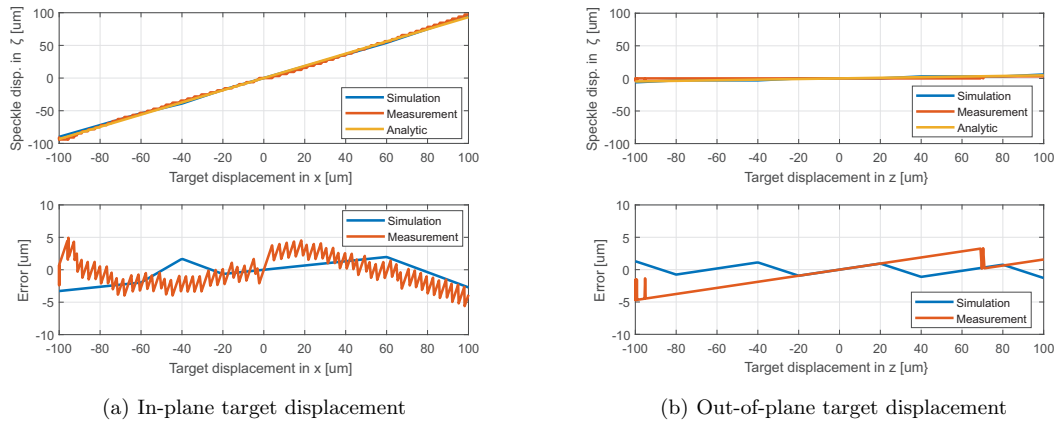


Figure 6. Simulation output (blue), experimentally measured (red) and analytic results (yellow) of the speckle pattern shift on the detector for the tilted laser setup. (a) shows the results for in-plane displacements of the target and the related errors with respect to the analytic result. (b) depicts the results for out-of-plane displacements.

The simulation results for the second setup with tilted detector (b) and the third setup with laser and detector tilted (c) are in the same range of accuracy as for the first setup (data not shown). The peak-to-valley and the rms errors for all setups are listed in Table 1. As predicted by theory, the sensitivity of the second setup for in-plane displacements is only about 60% of the first setup, while the crosstalk from out-of-plane displacement additionally increases by a factor of 10. The third setup shows a sensitivity which is about 80% of the first setup but also shows a crosstalk a factor 6 larger than the first setup. From this perspective the first setup is best suited for the design of sensors measuring the in-plane displacement of a target.

Table 1. Simulation error of OLSP setup for in-plane (IP) and out-of-plane (OOP) displacement of the target.

	Tilted laser		Tilted detector		Both tilted	
	IP	OOP	IP	OOP	IP	OOP
ptv error [ $\mu\text{m}$ ]	5.2	2.6	2.8	3.9	4.4	5.1
rms error [ $\mu\text{m}$ ]	1.9	0.9	1.0	1.2	1.4	1.1

For the fourth setup (see Fig. 5d) with additional aperture, the NCC peak shift is again evaluated as measure

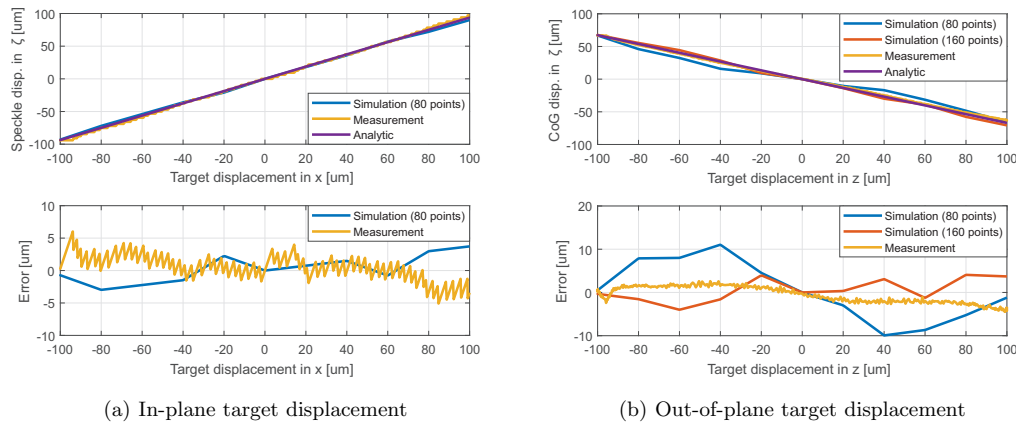


Figure 7. Simulation output for the integrated sensor setup with aperture. The result for 80 (blue) and 160 (red) point sources, the experimental data (yellow) and analytic results (violet) of (a) the speckle pattern shift for in-plane displacements and (b) the CoG shift on the detector for out-of-plane displacements are shown.

for in-plane displacement and the CoG shift is used as additional simulation output to determine the out-of-plane displacement of the target. For the analytic calculation of the CoG shift geometric relations based on the nominal setup assembly are used. For calculation of the NCC peak shift, the aperture is neglected and (1) is used. The simulation is again evaluated for target displacements of  $20 \mu\text{m}$  steps over a motion range of  $200 \mu\text{m}$  and relative to the reference at  $0 \mu\text{m}$  displacement. To demonstrate the relation between number of point sources and the achieved accuracy, the simulation is performed for 80 and 160 point sources. Fig. 7 shows the simulated, measured and analytically calculated values for both simulation outputs. The sensitivity to in-plane displacements, the crosstalk and the resulting simulation error is comparable to the first setup (see results without aperture in Fig. 6a), with the error being only insignificantly affected by the larger number of point sources. The resulting experimental sensitivity to out-of-plane displacements due to the CoG shift is  $0.67$  and matches the analytic value well. With 80 point sources significant deviations of about  $10 \mu\text{m}$  between simulated and analytic value can be observed for out-of-plane displacements around  $\pm 50 \mu\text{m}$ . Overall the simulation shows a peak-to-valley error of  $20.9 \mu\text{m}$  and an rms error of  $6.6 \mu\text{m}$  for out-of-plane displacements. Increasing the number of point sources to 160, the accuracy is significantly increased and the error decreases to  $8.1 \mu\text{m}$  peak-to-valley and  $2.6 \mu\text{m}$  rms, which again even lies below the resolution of the experimental setup. The accuracy improvement, however, comes at the cost of a doubled computation time.

In summary it is shown that the developed simulation tool is capable of accurately simulating speckle effects for various geometries of in-plane as well as integrated in- and out-of-plane sensors assemblies with resulting simulation errors of less than  $2 \mu\text{m}$  rms for NCC peak and  $2.6 \mu\text{m}$  rms for CoG shifts, respectively.

## 5. CONCLUSION

In this paper a versatile, accurate and efficient speckle simulation tool integrating the statistical nature of speckles with the deterministic properties of ray-tracing simulations is developed for the design of laser-based sensors. It enables the calculation of several simulation outputs, such as correlation peak shift, center of gravity shift or crosstalk, in order to determine the best performing sensor system configuration for a given requirement and measurement principle. The simulation tool is capable of considering the entire system geometry including the locations, orientation and size of the laser source, the target surface, the detector (with number and size of pixels) and apertures, mirrors or lenses, if applicable. The laser spot on the target is approximated by a sufficiently large number of individual point sources with random height distribution in the range of the surface roughness, where each point source is then simulated by  $N_2$  rays that are traced through the optical system and provide the respective intensity and phase at each detector pixel. The speckle image on the detector is



calculated by complex summation of the intensity and phase image matrix of all point sources on the detector. To validate the simulation results for various system geometries, they are compared against the experimental data and analytical results of four designed laser-speckle based sensor setups for measuring in- and out-of-plane displacements of a target. The resulting simulation errors for in-plane (output: correlation peak shift) and out-of-plane displacements (output: center of gravity shift) are in the range of  $2\ \mu\text{m}$  rms and  $2.6\ \mu\text{m}$  rms, respectively, demonstrating the good accuracy of the simulation tool already for a fair amount of point sources. Increasing the number of point sources is shown to reduce the error of the CoG shift output, while not affecting the NCC peak shift output, such that an individual tradeoff between computation time and accuracy is required for each sensor system design. Future work includes the advancement of the simulation tool in terms of computational efficiency and the application for uncertainty estimations of laser based sensor systems.

## REFERENCES

- [1] M. Ries, B. D. D. Senneville, S. Roujol, Y. Berber, B. Quesson, and C. Moonen, "Real-time 3d target tracking in mri guided focused ultrasound ablations in moving tissues," *Magnetic Resonance in Medicine* **64**(6), pp. 1704–1712, 2010.
- [2] A. Krupa, G. Fichtinger, and G. D. Hager, "Full motion tracking in ultrasound using image speckle information and visual servoing," *Proceedings 2007 IEEE International Conference on Robotics and Automation*, pp. 2458–2464, 2007.
- [3] M. Thier, R. Saathof, A. Sinn, R. Hainisch, and G. Schitter, "Six degree of freedom vibration isolation platform for in-line nano-metrology," *IFAC-PapersOnLine* **49**(21), pp. 149–156, 2016.
- [4] Y. Chen and F. Dong, "Robot machining: recent development and future research issues," *The International Journal of Advanced Manufacturing Technology* **66**(9-12), pp. 1489–1497, 2013.
- [5] D. Imkamp, R. Schmitt, and J. Berthold, "Blick in die zukunft der fertigungsmesstechnik - die vdi/vde-gma roadmap fertigungsmesstechnik 2020," *Technisches Messen* **10**(79), pp. 433–439, 2012.
- [6] D. Wertjanz, E. Csencsics, and G. Schitter, "3 dof vibration compensation platform for robot-based precision inline measurements on free-form surfaces," *IEEE Transactions on Industrial Electronics*, in press, 2021.
- [7] C. P. Keferstein and W. Dutschke, *Fertigungsmesstechnik*, Springer Vieweg, Wiesbaden, 2010.
- [8] P. Rastogi and D. Inaudi, eds., *Trends in Optical Non-Destructive Testing*, Elsevier Science, Kidlington, Oxford, England, 2000.
- [9] S. Schneider, Y. Gautam, and B. Zagar, "Application of a locally operating laser-speckle strain sensor," *IEEE Transactions on Instrumentation and Measurement* **52**(4), pp. 1025–1029, 2003.
- [10] I. Yamaguchi, T. Takemori, and K. Kobayashi, "Stabilized and accelerated speckle strain gauge," *Optical engineering* **32**(3), pp. 618–625, 1993.
- [11] T. O. Charrett, Y. K. Bandari, F. Michel, J. Ding, S. W. Williams, and R. P. Tatam, "A non-contact laser speckle sensor for the measurement of robotic tool speed," *Robotics and Computer-Integrated Manufacturing* **53**, pp. 187–196, 2018.
- [12] T. O. Charrett, T. Kissinger, and R. P. Tatam, "Workpiece positioning sensor (wpos): A three-degree-of-freedom relative end-effector positioning sensor for robotic manufacturing," *Procedia CIRP* **79**, pp. 620–625, 2019.
- [13] R. Paris, M. Melik-Merkumians, and G. Schitter, "Probabilistic absolute position sensor based on objective laser speckles," *IEEE Transactions on Instrumentation and Measurement* **65**(5), pp. 1188–1196, 2016.
- [14] E. Csencsics, "Integrated compensation-based laser sensor system for in-plane and out-of-plane target tracking," *Applied Optics* **59**(20), pp. 6138–6147, 2020.
- [15] R. G. Dorsch, G. Häusler, and J. M. Herrmann, "Laser triangulation: fundamental uncertainty in distance measurement," *Applied optics* **33**(7), pp. 1306–1314, 1994.
- [16] D. D. Duncan and S. J. Kirkpatrick, "The copula: a tool for simulating speckle dynamics," *JOSA A* **25**(1), pp. 231–237, 2008.
- [17] D. D. Duncan and S. J. Kirkpatrick, "Algorithms for simulation of speckle (laser and otherwise)," in *Complex Dynamics and Fluctuations in Biomedical Photonics V*, **6855**, p. 685505, International Society for Optics and Photonics, 2008.

- [18] A. Federico, G. Kaufmann, G. Galizzi, H. Rabal, M. Trivi, and R. Arizaga, "Simulation of dynamic speckle sequences and its application to the analysis of transient processes," *Optics Communications* **260**(2), pp. 493–499, 2006.
- [19] J. W. Goodman, "Some fundamental properties of speckle," *JOSA* **66**(11), pp. 1145–1150, 1976.
- [20] I. Yamaguchi, "Speckle displacement and decorrelation in the diffraction and image fields for small object deformation," *Optica Acta: International Journal of Optics* **28**(10), pp. 1359–1376, 1981.
- [21] M. Sjoedahl, "Calculation of speckle displacement, decorrelation, and object-point location in imaging systems," *Applied Optics* **34**(34), pp. 7998–8010, 1995.
- [22] M. Sjoedahl, "Accuracy in electronic speckle photography," *Applied Optics* **36**(13), p. 2875–2885, 1997.
- [23] Y. Petrov, "Optometrika - matlab library." Mathworks website: <https://de.mathworks.com/matlabcentral/fileexchange/45355-optometrika>, 2021.
- [24] R. Paris, T. Thurner, and G. Schitter, "Compensation based displacement measurement using objective laser speckles," *IFAC Proceedings Volumes* **46**(5), pp. 264–270, 2013.